Nanoscale

# Layer-by-layer Assembly of MXene and Carbon Nanotubes on Electrospun Polymer Films for Flexible Energy Storage



| | |
|---|---|
| Journal: | *Nanoscale* |
| Manuscript ID | NR-ART-01-2018-000313.R1 |
| Article Type: | Paper |
| Date Submitted by the Author: | 06-Feb-2018 |





| | |
|---|---|
| Complete List of Authors: | Zhou, Zehang; University of Pennsylvania, Materials Science and Engineering<br>Panatdasirisuk, Weerapha; University of Pennsylvania School of Arts and Sciences, Materials Science and Engineering<br>Mathis, Tyler ; Drexel University<br>Anasori , Babak; Drexel University, Materials Science and Engineering<br>Lu, Canhui; Sichuan University<br>Zhang, Xinxing; Sichuan University State Key Laboratory of Polymer Materials Engineering, State Key Laboratory of Polymer Materials Engineering<br>Liao, Zhiwei; University of Pennsylvania, Materials Science and Engineering<br>Gogotsi, Yury; Drexel University, Department of Materials Science & Engineering, and A. J. Drexel Nanomaterials Institute<br>Yang, Shu ; University of Pennsylvania, Materials Science and Engineering |
| | |

Nanoscale

ARTICLE

# Layer-by-layer Assembly of MXene and Carbon Nanotubes on Electrospun Polymer Films for Flexible Energy Storage

Received 00th January 20xx,
Accepted 00th January 20xx

DOI: 10.1039/x0xx00000x

www.rsc.org/

*Zehang Zhou[1,2], Weerapha Panatdasirisuk[1], Tyler S. Mathis[3], Babak Anasori[3], Canhui Lu[2], Xinxing Zhang[2], Zhiwei Liao[1], Yury Gogotsi[3,*] and Shu Yang[1,*]*

Free-standing, highly flexible and foldable supercapacitor electrodes were fabricated through spray-coating assisted layer-by-layer assembly of $Ti_3C_2T_x$ (MXene) nanoflakes together with multi-walled carbon nanotubes (MWCNTs) on electrospun polycaprolactone (PCL) fiber networks. The open structure of the PCL network and the use of MWCNTs as spacers not only limits the restacking of $Ti_3C_2T_x$ flakes, but also increases the accessible surface of the active materials, facilitating fast diffusion of electrolyte ions within the electrode. The composite electrodes have areal capacitance (30 – 50 mF/cm$^2$) comparable to other templated electrodes reported in literature, but showed significantly improved rate performance (14- 16 % capacitance retention at a scan rate of 100 V s$^{-1}$). Furthermore, the composite electrodes are flexible and foldable, demonstrating good tolerance against repeated mechanical deformation, including twisting and folding. Therefore, these tens of micron thick fiber electrodes will be attractive for applications in energy storage, electroanalytical chemistry, brain electrodes, electrocatalysis and other fields, where flexible freestanding electrodes with an open and accessible surface are highly desired.

## 1. Introduction

Flexible electrodes that are fractions of a millimeter in thickness can be used in a variety of applications in fields ranging from energy storage to brain electrodes and electrocatalysis. Among these, energy storage is probably the most important and obvious application. In particular, supercapacitors have attracted significant research interest for small and portable electronic devices due to their high-power densities and high charging and discharging rates.[1,2] They are typically categorized into two groups according to their energy storage mechanisms. The first type is electrical double-layer capacitors (EDLCs),[3,4] where electro-static charge storage is achieved by the separation of ions in a Helmholtz double layer at the surface of the electrode. The second is pseudocapacitors,[5] where charge is stored through Faradic redox reactions at the surface of the electrode. EDLCs typically have a low energy density, which limits their potential applications in thin-film devices, when the amount of active material is limited. In comparison, pseudocapacitors offer higher energy densities, but have shorter cycling lifetime.

Early transition metal carbides, nitrides, and carbonitrides,[6,7] such as $Mo_2C$, $Ti_3C_2$, $Nb_4C_3$, known as MXenes, are a growing class of two-dimensional (2D), inorganic materials that offer high conductivity (~8,000 S cm$^{-1}$ for $Ti_3C_2$),[8] high specific capacitance,[9] excellent mechanical properties, and ion intercalation behavior.[10,11] The presence of a variety of functional groups (e.g. O, OH, F - $T_x$ in the chemical formula of MXenes - e.g., $Ti_3C_2T_x$) on their surfaces makes them hydrophilic.[8,12] MXenes have shown promise for electrochemical energy storage appli-cations, with MXenes having specific capacitances better than all other reported carbon materials, including carbon nanotubes (CNTs) and graphene.[13] However, MXene flakes often face issues such as restacking during film fabrication due to their 2D nature.[14,15] The inadequate diffusion of electrolyte ions through the restacked nanosheets prevents full utilization of the active redox surfaces of MXenes, which in turn limits the maximum total energy that can be stored and their capacitance retention at high charge-discharge rates.[16,17] In general, 2D nanomaterials suffer from similar issues. A widely studied strategy to prevent restacking is to introduce interlayer spacers, for example, by incorporating transition metal oxides and CNTs between graphene layers.[18-20] Similarly, a sandwiched $Ti_3C_2T_x$/CNT hybrid membrane was fabricated through alternating filtration, resulting in better capacitive performance than a $Ti_3C_2T_x$/CNT membrane made by simple mixing.[21]

Despite the extensive research efforts, challenges remain in controlled and scalable production of flexible and foldable

1.Department of Materials Science and Engineering, University of Pennsylvania, 3231 Walnut Street, Philadelphia, PA 19104, USA. E-mail: S. Yang, shuyang@seas.upenn.edu
2.State Key Laboratory of Polymer Materials Engineering, Polymer Research Institute of Sichuan University, Chengdu 610065, P. R. China.
3.Department of Materials Science and Engineering, and A. J. Drexel Nanomaterials Institute, Drexel University, 3141 Chestnut Street, Philadelphia, PA 19104, USA. E-mail: Y. Gogotsi, gogotsi@drexel.edu.
† Footnotes relating to the title and/or authors should appear here.
Electronic Supplementary Information (ESI) available: [details of any supplementary information available should be included here]. See DOI: 10.1039/x0xx00000x

supercapacitor electrodes with high energy and power densities.[22,23] Among different techniques to produce flexible templates, electrospinning offers a simple, versatile, and high-yield process to create three-dimensional (3D) fibrous networks with fiber diameters ranging from nanometers to micrometers by jetting a charged polymer solution under a high electric field in a continuous fashion.[24,25] The robust interconnected fiber networks and large specific surface areas have led to the templated electrodes with superior specific capacitance,[26-28] and enhanced flexibility.[29,30] However, previous attempts at embedding MXene into eletrospun fibers resulted in low MXene mass loading (~1 wt%) with properties that would be unfit for applications in energy storage and electronics.[31]

In this study, we report on the fabrication of highly flexible and foldable supercapacitor electrodes by hierarchical assembly of MXene/CNT multilayers on electrospun nanofiber substrates. MXene and multi-walled carbon nanotubes (MWCNTs) of opposite charges were spray coated layer-by-layer (LbL) onto electrospun polycaprolactone (PCL) fibers. PCL is one of the most promising polymer materials for electrospinning, which has been widely studied as a scaffold material in many applications such as tissue engineering and bone-regeneration due to its biocompatibility and flexibility.[32, 33] The MXene used in this study was $Ti_3C_2T_x$, which was synthesized by etching the parent MAX phase $Ti_3AlC_2$ in an acidic, fluoride containing solution using previously reported methods.[8,12] The highly porous nature of the PCL fiber network together with MWCNTs as spacers prevents restacking of $Ti_3C_2T_x$ sheets during electrode preparation, while the hierarchical structure of the $Ti_3C_2T_x$/MWCNT increases surface area, facilitating transport and infiltration of electrolyte ions into the electrode. The resulting templated electrodes have areal capacitances from 30 to 80 mF/cm$^2$ at 10mV/s, with the total charge stored depending on the coating amount. Due to the open electrode structure, high capacitance retention at high charge-discharge rates (~15% at 100 V s$^{-1}$) was achieved for all the templated electrodes tested. Furthermore, the composite electrodes demonstrated superior mechanical properties, including high flexibility, foldability, and decent structural integrity after repeated (100 cycles) mechanical deformation, including twisting and folding.

## 2. Experimental

### 2.1 MXene synthesis

$Ti_3C_2T_x$ suspensions were prepared by etching $Ti_3AlC_2$ powder in 9M hydrochloric acid (HCl) aqueous solution containing dissolved LiF salt ($Ti_3AlC_2$: LiF = 1:1 wt./wt.). The etching solution was stirred at a constant temperature of 35°C for 24 h. Following the etching, the $Ti_3C_2T_x$ sediment was washed using deionized (DI) water, followed by centrifugation until the pH of supernatant was near neutral (pH ~6). Then the $Ti_3C_2T_x$ sediment was re-dispersed in DI water and bath sonicated for 1 h, followed by centrifugation at 3500 rpm for 1 h. The supernatant of the final centrifugation was used for all the work reported in this study to ensure the $Ti_3C_2T_x$ being used was completely delaminated. The resulting $Ti_3C_2T_x$ aq. solution (0.5 wt.%) was used directly for spray coating and for fabrication of the vacuum filtered film.

### 2.2 Electrospun polycaprolactone (PCL) nanofiber film

13 wt.% PCL particles and 2 wt.% Tween 80 (Sigma Aldrich) as surfactant were dissolved in a mixed solvent of 40:60 wt./wt. tetrahydrofuran and acetone (Fisher Scientific) under continuous stirring. In a typical electrospinning experiment, the polymer solution was held in a 12-mL syringe, which was connected to a stainless-steel needle (gauge 20, outer diameter = 0.965 mm) as nozzle. The flow rate of the polymer solution was 1.2 mL h$^{-1}$. A rotating drum (diameter=2 cm, rotating speed = 30 rpm) wrapped with aluminum foil was used as a collector. The distance between the tip of the needle and collector was set at 10 cm. A self-made power supply was used to generate an 8 kV DC voltage for electrospinning. The obtained electrospun PCL film was thoroughly washed by DI water twice followed by air-drying. The PCL film was then treated by oxygen plasma (HARRICK Plasma Cleaner/Sterilizer, 230 W) for 25 min, followed by being immersed in a 0.3 wt.% branched polyethyleneimine (PEI, Sigma Aldrich) aqueous solution for 6 h.

### 2.3 Amination of multi-wall carbon nanotubes (MWCNTs)

The surface functionalization of MWCNTs was carried out according to literature.[34] MWCNTs (0.2 g, Cheap Tubes) and branched PEI (1g) were mixed in 20 mL of N,N-dimethylformamide (DMF). This dispersion was sonicated at 120 W for 30 min, followed by continuous stirring at 50 °C for 3 days. The obtained suspension was filtered through a 0.20 µm nylon membrane (Whatman), and washed with 1 M HCl aqueous solution, 1 M sodium hydroxide (NaOH) aqueous solution, DI water, and methanol to remove excess PEI.

### 2.4 Layer-by-layer assembly of MWCNT/$Ti_3C_2T_x$/PCL composite membranes

The MWCNT/$Ti_3C_2T_x$/PCL composite membrane was prepared by spray-coating of negatively charged $Ti_3C_2T_x$ suspension and positively charged MWCNT suspension on PEI functionalized PCL film alternatively. $Ti_3C_2T_x$ aqueous suspension (5 mg mL$^{-1}$) was spray-coated on the surface of PCL membrane using an airbrush (Master, Model G22) for 10 s at a distance of 10 cm under 50 psi. After the coated membrane was thoroughly rinsed with DI water, followed by air-drying for 20 min using a commercial hair-drier, positively charged MWCNT suspension (2.5 mg mL$^{-1}$) was coated on the surface of $Ti_3C_2T_x$/PCL film using the airbrush under the same condition. This process was repeated to allow the LbL assembly.

The $Ti_3C_2T_x$/PCL and MWCNT/$Ti_3C_2T_x$/PCL composite membranes were calcined in a tube furnace at 500 $^o$C for 2h under argon atmosphere to remove PCL and obtain the corresponding hollow fibers.

### 2.5 Characterization

The morphology of the composite membranes was observed using a scanning electron microscope (JEOL 7500 F SEM) at 5.0 kV. Thermal gravimetric analysis (TGA) was performed on SDT Q600 (TA Instruments) in $N_2$ at a heating rate of 5 $^o$C min$^{-1}$ to evaluate the thermal stability of the samples. Here $N_2$ was chosen as the gas to avoid the oxidation of $Ti_3C_2T_x$. Tensile testing was performed on using an Intron Universal Tester at a

crosshead rate of 10 mm $min^{-1}$. The samples were cut into 20 ×10 mm rectangles for testing. Zeta potential was measured on a Delsa Nano C Particle Analyzer, Beckman Coulter.

**2.6 Electrochemistry**

All electrochemical tests were conducted using a 3-electrode set-up with the $Ti_3C_2T_x$ films or $Ti_3C_2T_x$/fiber composites acting as the working electrode with an overcapacitive activated carbon counter electrode and an aqueous silver/silver chloride (Ag/AgCl) reference electrode with 3.5 M potassium chloride (KCl) filling solution. Glassy carbon was used as the current collectors for both working and counter electrodes and the electrodes were separated by a ~25 µm thick surfactant coated polypropylene membrane (Celgard, USA). Degassed 1 M sulfuric acid ($H_2SO_4$) was used as the electrolyte in all tests. All measurements were performed on a Bio-Logic VMP3 potentiostat (Bio-Logic, France). Electrochemical impedance spectroscopy was performed by applying a 10 mV sinusoidal voltage signal to the cells at the resting potential, with frequencies ranging from 10 mHz to 200 kHz. Cyclic voltammetry was performed from scan rates of 10 mV $s^{-1}$ to 100 V $s^{-1}$. Capacitance values were calculated by integration of the discharge current of the cyclic voltammograms with respect to time (Equation 1):

$$\boldsymbol{C\left(F/g\right)} = (\int_0^t \boldsymbol{i\,dt})/(\boldsymbol{V} * \boldsymbol{A}) \quad (1)$$

where $C$ is the specific capacitance (normalized to the geometric area of the working electrode), $t$ is the discharge time, $i$ is the discharge current, $V$ is the voltage window, and $A$ is the area of the working electrode.

## 3. Results and discussion

LbL assembly is commonly used in nanofabrication processes for alternating deposition of two or more components onto a supporting substrate through electrostatic adsorption and hydrogen bonding.[35] In this study, electrospun PCL nanofibers (Fig. S1) served as a nanofibrous scaffold for the deposition of electrochemically active $Ti_3C_2T_x$ sheets while MWCNTs were used as interlayer spacers. Since the surface of $Ti_3C_2T_x$ is negatively charged after chemical etching, to assist LbL assembly we grafted a positively charged polymer, branched polyethyleneimine (PEI), onto the surfaces of both the PCL matrix and the MWCNTs. The detailed LbL assembly procedure is shown in Fig. 1. Since PCL is hydrophobic, we introduced the surfactant Tween 80 in the electrospinning solution to improve the hydrophilicity of the obtained fiber network.[36] Oxygen plasma treatment was further conducted to activate the hydroxyl groups and carboxyl groups at the PCL chain ends (Fig. 1a).[37] The treated PCL was immersed in branched PEI solution where PEI interacted with PCL through hydrogen bonding, making the PCL surface positively charged.[38] Likewise, MWCNTs were modified by PEI to be positively charged (Fig. 1b).[34] The obtained PEI grafted MWCNT (PEI-*g*-MWCNT) aqueous dispersion remained stable after several days as shown in Fig. 1c.

The layered $Ti_3C_2T_x$/MWCNTs coating were created by spray coating the electrospun PCL nanofibers in an alternating sequence to obtain the LbL structures as illustrated in Fig. 1d. Briefly, an aqueous suspension of negatively charged $Ti_3C_2T_x$ sheets (0.5 wt.%) was spray coated onto the PEI functionalized PCL fiber network using an airbrush for 10 s (Step 1), leaving a thin and continuous layer of $Ti_3C_2T_x$ flakes on the fiber surface after rinsing and drying (Steps 2 and 3). Then a solution of positively charged PEI-*g*-MWCNT was spray coated on top of the $Ti_3C_2T_x$ layer (Step 4), followed by rinsing and drying (Steps 5 and 6). The LbL process was repeated twice to produce double-layered coatings of $Ti_3C_2T_x$ and MWCNTs, and the sample was denoted as (MWCNT/$Ti_3C_2T_x$)2-PCL. The photographs of PEI treated PCL film before and after LbL assembly are shown in Fig. 1e. LbL assembly of MWCNT/$Ti_3C_2T_x$ on PCL fibers via conventional dip coating was also attempted. However, regional agglomeration was observed in the composite films (see Fig. S2). It has been reported that spray-assisted LbL assembly offers highly uniform and ultra-thin coatings on the individual fibers of porous substrates, which is consistent with our results.[39]

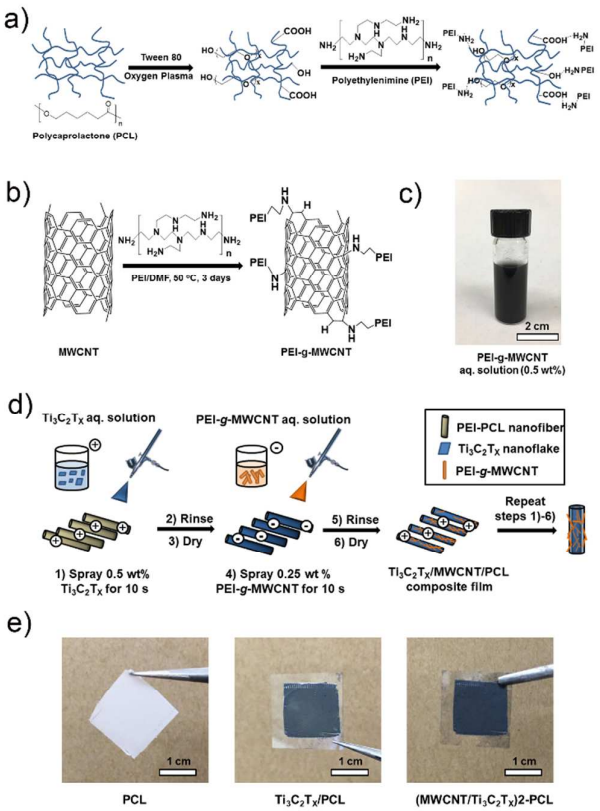


**Fig. 1.** (a) Schematic of the surface modification of PCL electro-spun fibers. (b) Illustration of direct amination of MWCNT with PEI. (c) The digital photograph of PEI-g-MWCNT dispersion after resting for 3 days. (d) Schematic illustrations of LbL spray coating process to fabricate hierarchical MWCNT/$Ti_3C_2T_x$ mul-tilayers on PCL fiber network. (e) The digital photographs of PEI/PCL, $Ti_3C_2T_x$/PCL and (MWCNT/$Ti_3C_2T_x$)2-PCL.

Additionally, the spray-assisted LbL approach significantly reduced the processing time in comparison to dip coating. In this study, only spray coated films were studied in detail. Zeta

potential measurement of $Ti_3C_2T_x$ (-31.33 mV), PEI aqueous solution (29.31 mV) and PEI-g-MWCNT dispersion (31.25 mV) indicates that the opposite polarities of the surface charges of the materials used for each spray coated layer enabled the grafting or absorption of the functional materials in the LbL assembly process.

The morphology of the composite nanofiber films was characterized by scanning electron microscopy (SEM) as shown in Fig. 2. The PEI treated PCL film has a nanofibrous structure

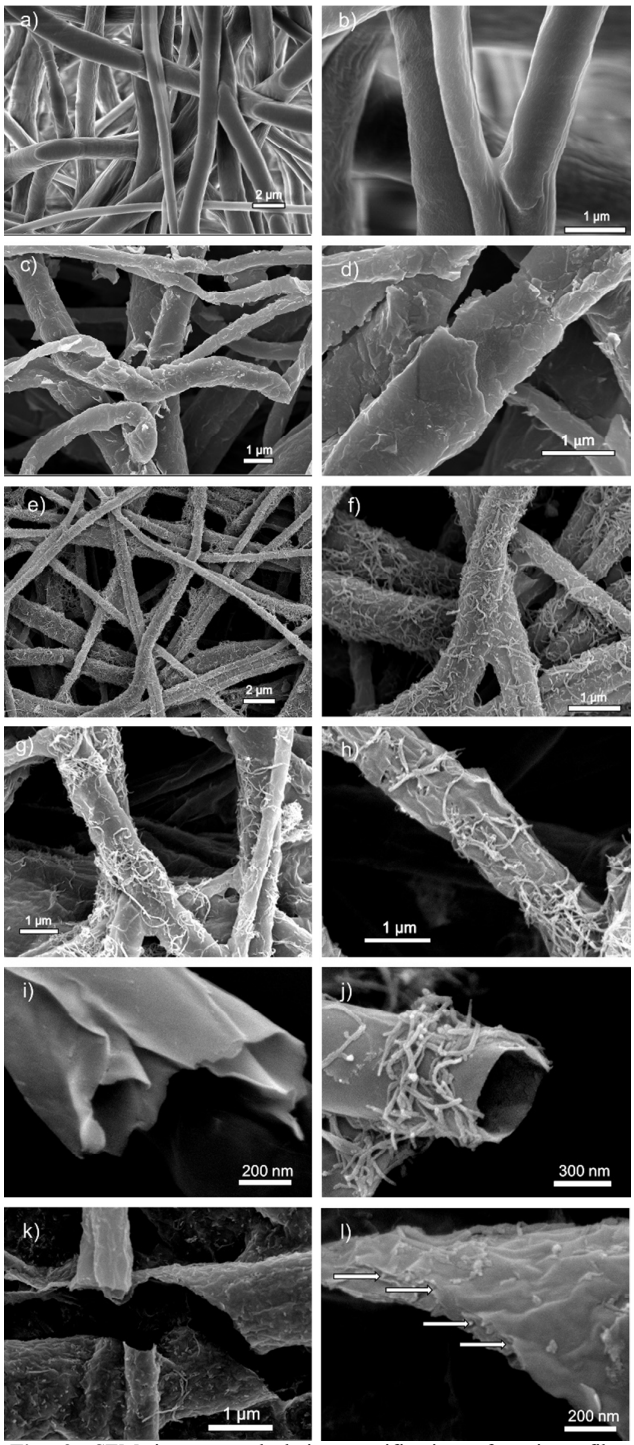


**Fig. 2.** SEM images and their magnification of various fiber networks. (a, b) PEI/PCL. (c, d) $Ti_3C_2T_x$/PCL. (e, f) MWCNT/$Ti_3C_2T_x$/PCL. (g, h) **(**MWCNT/ $Ti_3C_2T_x$)2-PCL. Samples shown in (i) $Ti_3C_2T_x$, (j) MWCNT/$Ti_3C_2T_x$, and (k-l) **(**MWCNT/$Ti_3C_2T_x$)2 composite hollow fiber films were prepared by annealing the samples at 500 $^oC$ for 2 h under argon. (l) Magnified image of (k). The interlayer spacing between $Ti_3C_2T_x$ layers separated by MWCNTs is indicated by white arrows.

identical to the pristine PCL fiber mats (see Fig. S1) with fiber diameters ranging from 500 nm to 1 μm as shown in Fig. 2a-b. After the deposition of $Ti_3C_2T_x$ nanosheets, the originally smooth PCL fibers became wrinkled and flaky (Fig. 2c-d), indicating that $Ti_3C_2T_x$ flakes were coated on the PCL template (Fig. 2c). Likewise, one-dimensional (1D) MWCNTs were uniformly deposited on the surface of $Ti_3C_2T_x$/PCL fibers through spray coating without severe agglomeration (Fig. 2e-f). Fig. 2g and 2h show the morphology of an LbL assembled $Ti_3C_2T_x$/MWCNT bilayer film after two coating cycles, referred to as (MWCNT/$Ti_3C_2T_x$)2-PCL; no major structural differences from that of one bilayer coating (MWCNT/$Ti_3C_2T_x$/ PCL) can be seen, where $Ti_3C_2T_x$ and MWCNTs wrapped around the surface of the PCL nanofibers uniformly. The successful coating of the $Ti_3C_2T_x$ and MWCNT and their morphology on PCL template was further confirmed after removal of the supporting PCL scaffold in a tube furnace at 500 °C for 2 h under argon. Hollow fiber structures can be seen in Fig. 2i-l. The results suggest that $Ti_3C_2T_x$ flakes formed a continuous and thin (~10 nm) self-supporting structure on the surface of PEI treated electrospun PCL fibers through spray coating, which would not collapse after removal of the polymer template. With the deposition of MWCNTs, the structure of bilayer and double-bilayer MWCNT/$Ti_3C_2T_x$ coating was well-maintained. The MWCNTs layer also served as an interlayer spacer (indicated by white arrows in Fig. 2l) separating the $Ti_3C_2T_x$ flakes (Fig. 2k and l) to limit restacking. However, when the number of spray coating cycles was increased to 3 and higher, local agglomeration of $Ti_3C_2T_x$ and MWCNTs was observed, blocking the pores of the PCL network (see Fig. S3). Therefore, the electrochemistry study reported here is based on two coating cycles to avoid agglomeration.

Since our end goal is to prepare flexible and foldable electrodes, the mechanical strength and flexibility of the $Ti_3C_2T_x$/fiber composite electrodes is crucial to their potential applications in wearable and portable energy storage devices. While many MXene and MXene-based composite films have been reported as electrodes for energy storage devices,[40] little has been shown about their conductivity after mechanical deformations, such as bending and twisting. We previously reported synthesis of triple interpenetrating networks of CNT/polyaniline on macroporous cellulose fibers as flexible and foldable supercapacitor electrodes with good mechanical integrity.[41] Here, we expect the nonwoven PCL electrospun fiber networks in this study should also provide a flexible and foldable scaffold to host a thin layer of $Ti_3C_2T_x$ and MWCNTs.

Stress-strain curves for the $Ti_3C_2T_x$/fiber composites are shown in Fig. 3. After the deposition of $Ti_3C_2T_x$ nanoflakes, the strain at the breaking point of the electrospun film decreased from 111.9% to 82.0%, attributed to stiffening of the structure after deposition of $Ti_3C_2T_x$. Consistently, the tensile strength of the composite membranes increased from 2.2 MPa to 3.0 MPa, as the result of the large interfacial interactions between the rigid 2D nanomaterials and the polymer matrix.[42]

We repeatedly folded or twisted the (MWCNT/$Ti_3C_2T_x$)2-PCL composite films (60 μm thick) up to 100 times. We then assembled the deformed film to build a circuit to illuminate an LED light (see Fig. 4a-c). The surface resistance was measured

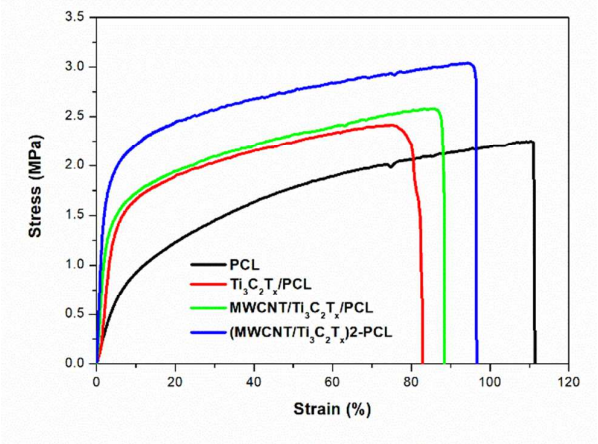


**Fig. 3.** Typical stress-strain curves of the electrospun PCL film, $Ti_3C_2T_x$/PCL, MWCNT/$Ti_3C_2T_x$/PCL and (MWCNT/$Ti_3C_2T_x$)2 -PCL composite films.

using a multimeter with a probe separation of 10 mm. The resistance values of the pristine $Ti_3C_2T_x$/PCL, MWCNT/$Ti_3C_2T_x$/PCL, and (MWCNT/$Ti_3C_2T_x$)2-PCL composite films were 1,700, 900 and 500 Ω, respectively. After folding and twisting for 100 times each, the resistance of the (MWCNT/$Ti_3C_2T_x$)2-PCL films increased from 500 Ω to 1,100 Ω and 1,300 Ω, respectively. Likewise, the resistance of the repeatedly deformed $Ti_3C_2T_x$/PCL films increased from 1,700 Ω to 4,800 Ω (folded) and 5,500 Ω (twisted), respectively, while the resistance of deformed MWCNT/$Ti_3C_2T_x$/PCL films increased from 900 Ω to 3,500 Ω (folded) and 4,200 Ω (twisted), respectively. Nevertheless, all the composite films remained to be sufficiently conductive that no noticeable changes of the blue LED light intensity could be discerned by the naked eyes (see Fig. 4b-c). Closer examination by SEM shows that most of the MWCNT/$Ti_3C_2T_x$ coated PCL fibers in the (MWCNT/$Ti_3C_2T_x$)2-PCL film remained intact after folding or twisting; only a few of them were fractured (Fig. S4). We believe the strong interactions between the functional groups of MXenes and the polymer scaffold, together with the high flexibility of the supporting electrospun fiber network, contributed to the overall structural integrity after repeated mechanical deformation. Furthermore, 1D MWCNTs served as conductive bridges connecting $Ti_3C_2T_x$ sheets, which also improved the tolerance of the conductive pathway against deformation. Fig. 4d shows a folded airplane made from a (MWCNT/$Ti_3C_2T_x$)2-PCL electrospun composite, further demonstrating its flexibility.

The templated $Ti_3C_2T_x$/PCL/MWCNT composites were then tested as supercapacitor electrodes using sulfuric acid ($H_2SO_4$) electrolyte, and representative cyclic voltammograms (CVs) and the rate performance for the composite films are shown in Fig. 5a and b, respectively. We chose an acidic electrolyte due to the high ionic conductivity and excess protons that are known to participate in redox reactions in transition-metal oxides and MXenes, which contributes to the overall

capacitance via fast, Faradaic reactions at the surface of the material.[9] At a scan rate of 10 mV/s, all the CVs show the characteristic charge-discharge behavior of $Ti_3C_2T_x$, where there is combination of a rectangular regime and a pair of pronounced broad and reversible redox peaks. The discrepancy in areal capacitance for the MWCNT/Ti3C2Tx coated electrodes in different cycles of spray coating is likely attributed to variance in loading of active materials in the spray coater, which is especially challenging when the amount of active materials is very small for an ultrathin coating, and intrinsic randomness in depositing materials on a target by the spray coating process. The problem could be alleviated by careful design of an automated spray coater in a controlled environment. However, we believe that this is beyond the scope of this study.

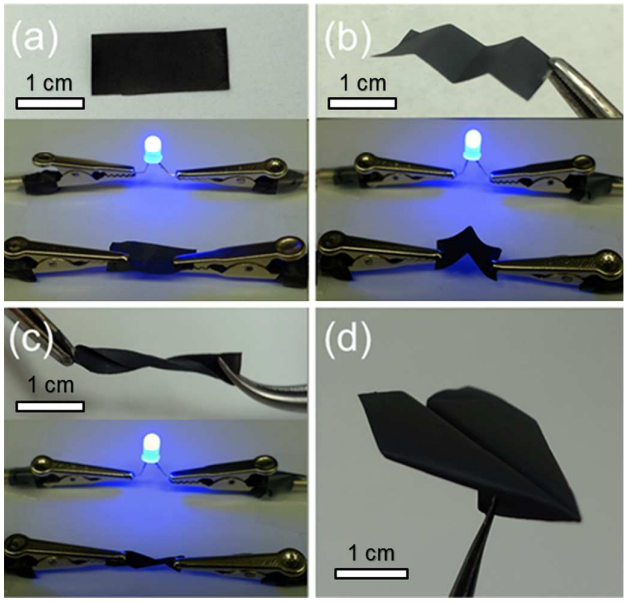


**Fig. 4.** Digital images of (a) the pristine, (b) folded, and (c) twisted (up to 100 times) **(**$MWCNT/Ti_3C_2T_x$)2-PCL films and the corresponding circuits built from them to light up a blue LED. (d) The composite film is folded into an airplane, demonstrating its flexibility.

When comparing the cycling stability of the $Ti_3C_2T_x$/fiber composite electrode to that of the vacuum filtered $Ti_3C_2T_x$ electrode (Fig. 5f), it can be seen that increasing the coating cycle to 2, and thus the amount of $MWCNT/Ti_3C_2T_x$ on the template helped to extend the lifetime of the composite electrodes. The improved cycling stability is attributed to the construction of interconnected structures, where $Ti_3C_2T_x$ was electrostatically bonded to PEI modified MWCNTs. The interconnected structure helped to protect the conductive layers and PCL matrix from collapse during repeated charging/discharging process. When the spray coating cycle was increased to three and more, while the total amount of MXene and the total charge stored were increased, regional agglomeration of $MWCNT/Ti_3C_2T_x$ on PCL aggravated on the polymer support (Fig. S3). As a result, the cycling lifetime (Fig. S5) and overall electrochemical performance for the $(MWCNT/Ti_3C_2T_x)$3-PCL film (3 cycles of bilayer coating) decreased (Fig. S6). This is not the case for $Ti_3C_2T_x$/PCL, $MWCNT/Ti_3C_2T_x$/PCL and $(MWCNT/Ti_3C_2T_x)$2-PCL composite membranes, which had rather uniform coatings of $Ti_3C_2T_x$ and MWCNTs. We note that when the electrode capacitance falls below 80% relative to the first cycle, the electrodes are considered to have reached the end of their lifetime.

The capacitive performance for the $Ti_3C_2T_x$/fiber composite film electrodes is compared to that of a vacuum filtered $Ti_3C_2T_x$ film electrode in Fig. S6. When the scan rate was increased to 1 V/s, there were negligible distortions in the CVs of all the $MWCNT/Ti_3C_2T_x$/PCL composites (Fig. S6c), which demonstrates the high rate capability of the composite electrodes. To contrast, the cyclic voltammogram of the pristine $Ti_3C_2T_x$ film was severely distorted when the scan rate was increased to 1V/s (Fig. S6a). The improved electrolyte accessibility to $Ti_3C_2T_x$ on the electrospun fiber templates was also evident by comparing the rate handling performance of the electrodes made from the $Ti_3C_2T_x$/fiber composite films vs. the vacuum filtered $Ti_3C_2T_x$ film. The improved capacitance retention of the templated electrodes indicate that the highly porous $Ti_3C_2T_x$/PCL structure effectively inhibits the restacking of $Ti_3C_2T_x$ nanoflakes, while the highly accessible active surfaces of the templated electrodes facilitate the transport of the electrolyte ions within the electrodes.

Fig. 5c shows Nyquist plots for each of the electrode materials. A low real-axis intercept value (< 0.4 $\Omega*cm^{-2}$ for each electrode) indicates low series resistance, which is expected for $Ti_3C_2T_x$ electrodes. The plot for each electrode material is nearly vertical

in the low-frequency region, indicating close to ideal capacitive behaviors for thin layers of $Ti_3C_2T_x$ exposed to the electrolyte. Since nearly all the active material is exposed to the electrolyte, the electrode/electrolyte resistance (ohmic solution resistance) and ohmic interparticle resistance is minimized by the uniformity of the coating; both factors lead to the electrodes being close to ideally polarizable.

The lack of any noticeable semi-circle in the high frequency regions of all the electrodes indicates that there is little to no charge transfer resistance for any of the electrodes, which is typical for MXenes when tested in an acidic electrolyte.[9,13,21] The most noteworthy difference between the $Ti_3C_2T_x$/fiber composite electrodes and the pristine $Ti_3C_2T_x$ film electrode can be seen in the mid-frequency region. For the $Ti_3C_2T_x$ film electrode, the resistance values are shifted towards more positive values, suggesting that the electrolyte ions are not able to access the entirety of the layered $Ti_3C_2T_x$ structure.[43] This limitation is not seen for any of the $Ti_3C_2T_x$/fiber composite electrodes, consistent with the reasoning behind the improvements seen in the high rate handing abilities of the $Ti_3C_2T_x$/fiber electrodes.

To evaluate the gravimetric charge storage of the composite electrodes we attempted to determine the loading amount of $Ti_3C_2T_x$ and MWCNT by measuring the thermal stability of the composite films using thermal gravimetric analysis (TGA). Based on the solid residue of $Ti_3C_2T_x$, MWCNT (~100 wt% as a carbon material), and PEI grafted PCL at 600 $^oC$, we calculated the mass loading of $Ti_3C_2T_x$/MWCNT for each composite film and the results are summarized in Table S1. When comparing the mass loading calculated by TGA to the areal capacitances of the composite electrodes (Fig. 5 and Fig. S6), we find that the calculated values do not follow the trend expected from the capacitance values. We attribute the discrepancies to the small

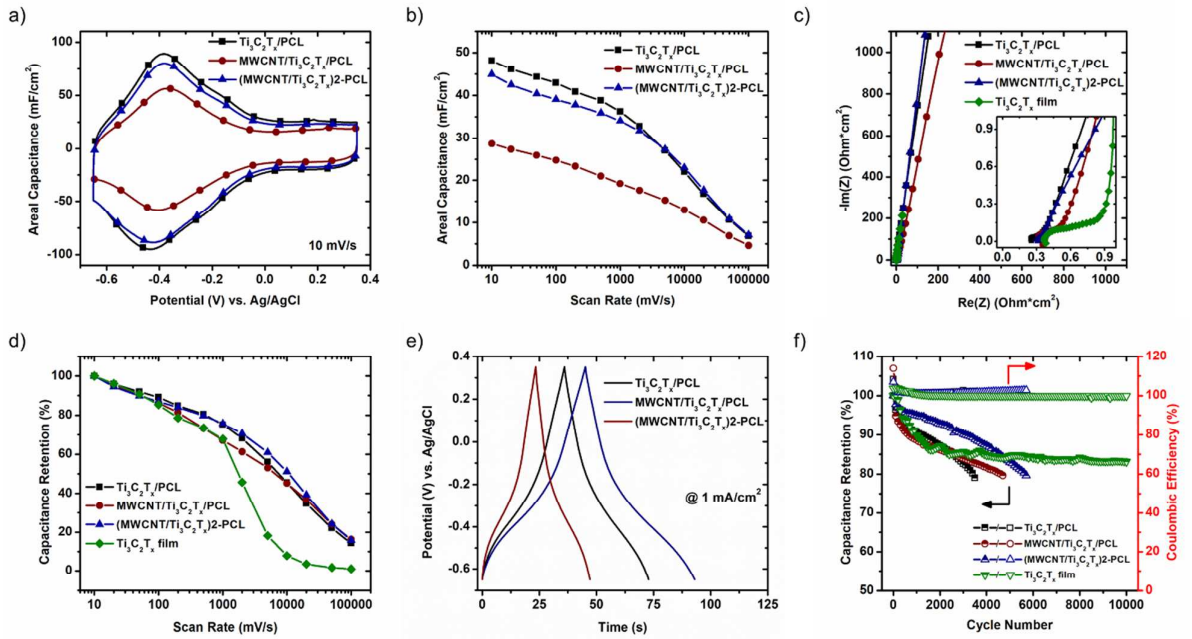


**Fig. 5.** (a) Cyclic voltammograms of the $Ti_3C_2T_x$/PCL, MWCNT/$Ti_3C_2T_x$/PCL, and (MWCNT/$Ti_3C_2T_x$)2-PCL composite electrodes in 1 M $H_2SO_4$ electrolyte at a scan rate of 10 mV/s. (b) Rate handling plot for the composite electrodes. (c) Nyquist plots of the composite films vs. the pristine $Ti_3C_2T_x$ film as electrodes. Inset: the high-frequency region of the plot. (d) Capacitance retention as a function of scan rate for the composite electrodes vs. the pristine $Ti_3C_2T_x$ film electrode. (e) Galvanostatic charge-discharge curves for the composite electrodes at a current density of 1 mA/cm$^2$. (f) Capacitance retention and coulombic efficiency vs. cycle numbers for the composite electrodes and the pristine $Ti_3C_2T_x$ film electrode.

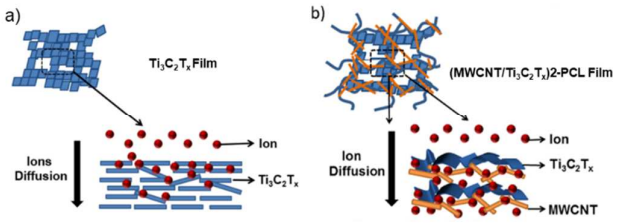


**Fig. 6.** Schematic illustrations of the ion diffusion in a $Ti_3C_2T_x$ film (a) and a (MWCNT/$Ti_3C_2T_x$)2-PCL film (b).

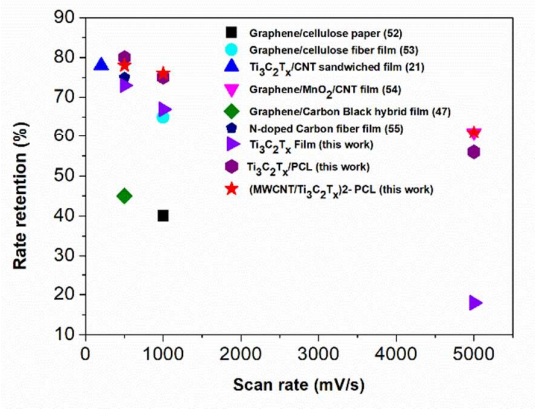


**Fig. 7.** Summary of electrochemical performance of different flexible electrodes in terms of rate retention.

amount of active material present on the PCL scaffold and the possibility that PCL was not completely removed, leaving carbonized residual. Therefore, the mass loading calculated by TGA was an estimate. Nevertheless, we calculated the gravimetric capacitance of the MXene/PCL composites using the mass loading values from Table S1 (see results shown in Fig. S7). At such mass loading values, we should expect similar gravimetric performance for each composite electrode. Here, because of the discrepancies men-tioned earlier, the gravimetric values of the different composite electrodes shown here are mainly to confirm that they are in the expected range for charge storage. Fig. S8 shows the full weight loss profiles of each material. The PEI treated PCL membrane showed monotonic weight loss starting at ~350 $^{o}$C as a result of the decomposition of PCL.[44] Majority of PCL was decomposed when the temperature reached ~450 $^{o}$C. A pristine $Ti_3C_2T_x$ film prepared by vacuum filtration was prepared and used for comparison. The latter showed ~10 % weight loss up to 600 $^{o}$C, mainly due to the loss of water from the $Ti_3C_2T_x$ interlayers and the removal of surface functional groups.[45,46] The weight loss of the $Ti_3C_2T_x$ coated PCL composite ($Ti_3C_2T_x$/PCL) started at ~280 $^{o}$C, lower than that of the pristine PEI grafted PCL film. This may be attributed to unfavorable interactions between $Ti_3C_2T_x$ and PCL at elevated temperatures leading to accelerated weight loss.

The MWCNTs in the layered composite films helped to create separation between the $Ti_3C_2T_x$ layers (as indicated by arrows in Fig. 2l), which can be clearly seen by the morphology of the annealed (MWCNT/$Ti_3C_2T_x$)2-PCL hollow fibers. The incorporation of this type of interlayer spacers improved electrolyte access during the charge/discharge process, which in turn partially overcome the issue of restacking of the $Ti_3C_2T_x$ nanoflakes and facilitated diffusion of electrolyte ions to the inner regions of the electrode as depicted in Fig. 6. As a result, the capacitance retention of the composite fiber electrode was higher than that of the vacuum filtered $Ti_3C_2T_x$ film at high scan rates. Furthermore, our composite electrodes showed improved capacitance retention relative to other nanostructured electrodes reported in the literature, as shown in Fig. 7.[47-49] The synergistic effects of the use of 2D $Ti_3C_2T_x$ nanoflakes, the highly accessible surface area of the electrospun nanofibrous scaffold, and the hierarchical nanostructure constructed through LbL assembly significantly increased the accessibility and diffusion of electrolyte ions to the active materials. Overall, being free-standing and binder-free electrodes, our composite films offer comparable capacitance but improved rate retention relative to reports in the literature for similar nanofiber supported electrodes.

## 4. Conclusion

In summary, we developed a simple LbL assembly process via spray coating of $Ti_3C_2T_x$ and MWCNT on electrospun PCL nanofiber networks to form templated electrodes. $Ti_3C_2T_x$ nanosheets and MWCNTs were uniformly deposited on PCL fiber substrates and the obtained free-standing composite films were tested as supercapacitor electrodes. The composite films showed capacitance retentions of 14-16 % of their initial capacitance when the scan rate was increased from 10 mV $s^{-1}$ to 100 V $s^{-1}$ vs. just 1% capacitance retention for a standard vacuum filtered $Ti_3C_2T_x$ film electrode. The highly porous and accessible morphology of the fiber network and the hierarchical structure of these $Ti_3C_2T_x$/fiber composite film electrodes together with the intrinsic high capacitance of MXene contributed to their overall charge storage and high rate performance. The composite films were highly flexible: they maintained their structural integrity and high conductivity during 100 cycles of folding or twisting. The spray-assisted LbL nanotemplating strategy offers the first step toward high performance, flexible, wearable, and portable MXene-based electrodes for energy-storage devices. These films may also find applications including electrocatalysis,[50] sensing,[51] and electromagnetic interference (EMI) shielding,[12] where thin and flexible conducting films with the maximum exposure of MXene to the environment are needed.

## Conflicts of interest

There are no conflicts to declare.

## Acknowledgements

Z.Z. was supported by the China Scholarship Council (Grant No. 201506240046). Material manufacturing was supported by the National Science Foundation (NSF)/EFRI-ODISSEI program, #EFRI 13-31583 (SY). Electrochemical characterization was supported by the Fluid Interface Reactions, Structures and Transport (FIRST) Center, an Energy Frontier Research Center funded by the U.S. Department of Energy, Office of Science, Basic Energy Sciences (YG).

## References

1. P. Simon and Y. Gogotsi, *Nat Mater*, 2008, **7**, 845-854.

2. B. E. Conway, *Electrochemical supercapacitors: scientific fundamentals and technological applications*, Springer Science & Business Media2013.
3. Y. Zhai, Y. Dou, D. Zhao, P. F. Fulvio, R. T. Mayes and S. Dai, *Adv. Mater.*, 2011, **23**, 4828-4850.
4. G. Wang, L. Zhang and J. Zhang, *Chem. Soc. Rev.*, 2012, **41**, 797-828.
5. H. Wang, H. S. Casalongue, Y. Liang and H. Dai, *J. Am. Chem. Soc.*, 2010, **132**, 7472-7477.
6. M. Naguib, O. Mashtalir, J. Carle, V. Presser, J. Lu, L. Hultman, Y. Gogotsi and M. W. Barsoum, *ACS Nano*, 2012, **6**, 1322-1331.
7. B. Anasori, M. R. Lukatskaya and Y. Gogotsi, *Nat. Rev. Mater.*, 2017, **2**, 16098.
8. M. Alhabeb, K. Maleski, B. Anasori, P. Lelyukh, L. Clark, S. Sin and Y. Gogotsi, *Chem. Mater.*, 2017, **29**, 7633-7644.
9. M. R. Lukatskaya, S. Kota, Z. Lin, M.-Q. Zhao, N. Shpigel, M. D. Levi, J. Halim, P.-L. Taberna, M. W. Barsoum, P. Simon and Y. Gogotsi, *Nat. Energy*, 2017, **2**, 17105.
10. M. R. Lukatskaya, S.-M. Bak, X. Yu, X.-Q. Yang, M. W. Barsoum and Y. Gogotsi, *Adv. Energy Mater.*, 2015, **5**, 1500589-n/a.
11. R. B. Rakhi, B. Ahmed, M. N. Hedhili, D. H. Anjum and H. N. Alshareef, *Chem. Mater.*, 2015, **27**, 5314-5323.
12. F. Shahzad, M. Alhabeb, C. B. Hatter, B. Anasori, S. Man Hong, C. M. Koo and Y. Gogotsi, *Science*, 2016, **353**, 1137-1140.
13. M. Ghidiu, M. R. Lukatskaya, M.-Q. Zhao, Y. Gogotsi and M. W. Barsoum, *Nature*, 2014, **516**, 78-81.
14. X. Xie, M.-Q. Zhao, B. Anasori, K. Maleski, C. E. Ren, J. Li, B. W. Byles, E. Pomerantseva, G. Wang and Y. Gogotsi, *Nano Energy*, 2016, **26**, 513-523.
15. Y. Han, X. Zhang, X. Wu and C. Lu, *ACS Sus. Chem. Engineering*, 2015, **3**, 1853-1859.
16. Q. Wang, J. Yan, Y. Wang, T. Wei, M. Zhang, X. Jing and Z. Fan, *Carbon*, 2014, **67**, 119-127.
17. Y. Li, Z. Li and P. K. Shen, *Adv. Mater.*, 2013, **25**, 2474-2480.
18. Z. Fan, J. Yan, L. Zhi, Q. Zhang, T. Wei, J. Feng, M. Zhang, W. Qian and F. Wei, *Adv. Mater.*, 2010, **22**, 3723-3728.
19. Z. Zhang, F. Xiao, L. Qian, J. Xiao, S. Wang and Y. Liu, *Adv. Energy Mater.*, 2014, **4**, 1400064-n/a.
20. J. Yan, Q. Wang, T. Wei and Z. Fan, *Adv. Energy Mater.*, 2014, **4**, 1300816-n/a.
21. M.-Q. Zhao, C. E. Ren, Z. Ling, M. R. Lukatskaya, C. Zhang, K. L. Van Aken, M. W. Barsoum and Y. Gogotsi, *Adv. Mater.*, 2015, **27**, 339-345.
22. X. Lang, A. Hirata, T. Fujita and M. Chen, *Nat Nano*, 2011, **6**, 232-236.
23. C. Choi, J. A. Lee, A. Y. Choi, Y. T. Kim, X. Lepró, M. D. Lima, R. H. Baughman and S. J. Kim, *Adv. Mater.*, 2014, **26**, 2059-2065.
24. C.-L. Zhang and S.-H. Yu, *Chem. Soc. Rev.*, 2014, **43**, 4423-4448.
25. F. Ko, Y. Gogotsi, A. Ali, N. Naguib, H. Ye, G. L. Yang, C. Li and P. Willis, *Adv. Mater.*, 2003, **15**, 1161-1165.
26. L. Deng, R. J. Young, I. A. Kinloch, A. M. Abdelkader, S. M. Holmes, D. A. De Haro-Del Rio and S. J. Eichhorn, *ACS Appl. Mater. Interfaces*, 2013, **5**, 9983-9990.
27. Z. Zhou and X.-F. Wu, *J. Power Sources*, 2013, **222**, 410-416.
28. Y. Gao, V. Presser, L. Zhang, J. J. Niu, J. K. McDonough, C. R. Pérez, H. Lin, H. Fong and Y. Gogotsi, *J. Power Sources*, 2012, **201**, 368-375.
29. S. Cavaliere, S. Subianto, I. Savych, D. J. Jones and J. Roziere, *Energ. Environ. Sci.*, 2011, **4**, 4761-4785.
30. Y.-E. Miao, W. Fan, D. Chen and T. Liu, *ACS Appl. Mater. Interfaces*, 2013, **5**, 4423-4428.
31. E. A. Mayerberger, O. Urbanek, R. M. McDaniel, R. M. Street, M. W. Barsoum and C. L. Schauer, *J. Appl. Polym. Sci.*, 2017, **134**, 45295-n/a.
32. P. Wutticharoenmongkol, N. Sanchavanakit, P. Pavasant and P. Supaphol, *Macromol. Biosci.*, 2006, **6**, 70-77.
33. J. Song, H. Gao, G. Zhu, X. Cao, X. Shi and Y. Wang, *Carbon*, 2015, **95**, 1039-1050.
34. K.-S. Liao, A. Wan, J. D. Batteas and D. E. Bergbreiter, *Langmuir*, 2008, **24**, 4245-4253.
35. D. S. Liu, J. N. Ashcraft, M. M. Mannarino, M. N. Silberstein, A. A. Argun, G. C. Rutledge, M. C. Boyce and P. T. Hammond, *Adv. Funct. Mater.*, 2013, **23**, 3087-3095.
36. W. Panatdasirisuk, Z. Liao, T. Vongsetskul and S. Yang, *Langmuir*, 2017, **33**, 5872-5878.
37. B. Gupta, K. Krishnanand and B. L. Deopura, *Eur. Polym. J.* 2012, **48**, 1940-1948.
38. Y. Ramgopal, D. Mondal, S. Venkatraman, W. Godbey and G. Yuen, *J. Biomed. Mater. Res. B.*, 2009, **89**, 439-447.
39. K. C. Krogman, J. L. Lowery, N. S. Zacharia, G. C. Rutledge and P. T. Hammond, *Nat Mater*, 2009, **8**, 512-518.
40. Q. Tang, Z. Zhou and P. Shen, *J. Am. Chem. Soc.*, 2012, **134**, 16909-16916.
41. D. Ge, L. Yang, L. Fan, C. Zhang, X. Xiao, Y. Gogotsi and S. Yang, *Nano Energy*, 2015, **11**, 568-578.
42. W. Shao, J. He, F. Sang, Q. Wang, L. Chen, S. Cui and B. Ding, *Mater. Sci. Eng. C*, 2016, **62**, 823-834.
43. P. L. Taberna, P. Simon and J. F. Fauvarque *J. Electrochem. Soc.*, 2003, **150**, A292-A300.
44. M. F. Canbolat, A. Celebioglu and T. Uyar, *Colloids Surfaces B*, 2014, **115**, 15-21.
45. M. Mariano, O. Mashtalir, F. Q. Antonio, W.-H. Ryu, B. Deng, F. Xia, Y. Gogotsi and A. D. Taylor, *Nanoscale*, 2016, **8**, 16371-16378.
46. O. Mashtalir, M. R. Lukatskaya, A. I. Kolesnikov, E. Raymundo-Pinero, M. Naguib, M. W. Barsoum and Y. Gogotsi, *Nanoscale*, 2016, **8**, 9128-9133.
47. Y. Wang, J. Chen, J. Cao, Y. Liu, Y. Zhou, J.-H. Ouyang and D. Jia, *J. Power Sources*, 2014, **271**, 269-277.
48. Y. Huang, J. Tao, W. Meng, M. Zhu, Y. Huang, Y. Fu, Y. Gao and C. Zhi, *Nano Energy*, 2015, **11**, 518-525.
49. Y. Gao, Y. S. Zhou, M. Qian, X. N. He, J. Redepenning, P. Goodman, H. M. Li, L. Jiang and Y. F. Lu, *Carbon*, 2013, **51**, 52-58.
50. Z. W. Seh, K. D. Fredrickson, B. Anasori, J. Kibsgaard, A. L. Strickler, M. R. Lukatskaya, Y. Gogotsi, T. F. Jaramillo and A. Vojvodic, *ACS Energy Letters*, 2016, **1**, 589-594.
51. H. Liu, C. Duan, C. Yang, W. Shen, F. Wang and Z. Zhu, *Sensors Actuat. B: Chem.*, 2015, **218**, 60-66.
52. Z. Weng, Y. Su, D.-W. Wang, F. Li, J. Du and H.-M. Cheng, *Adv. Energy Mater.*, 2011, **1**, 917-922.
53. L. Liu, Z. Niu, L. Zhang, W. Zhou, X. Chen and S. Xie, *Adv. Mater.*, 2014, **26**, 4855-4862.
54. Y. Cheng, S. Lu, H. Zhang, C. V. Varanasi and J. Liu, *Nano Letters*, 2012, **12**, 4206-4211.
55. C. Long, D. Qi, T. Wei, J. Yan, L. Jiang and Z. Fan, *Adv. Funct. Mater.*, 2014, **24**, 3953-3961.

TOC graphics

## Layer-by-layer Assembly of MXene and Carbon Nanotubes on Electrospun Polymer Films for Flexible Energy Storage

*Zehang Zhou[1,2], Weerapha Panatdasirisuk[1], Tyler S. Mathis[3], Babak Anasori[3], Canhui Lu[2], Xinxing Zhang[2], Zhiwei Liao[1], Yury Gogotsi[3,*] and Shu Yang[1,*]*

Free-standing, highly flexible and foldable supercapacitor electrodes were fabricated by spray-assisted layer-by-layer assembly of $Ti_3C_2T_x$ (MXene) nanoflakes with multi-walled carbon nanotubes (MWCNTs) on electrospun polycaprolactone (PCL) fiber networks.